6-2013

Meter-Sized Moonlet Population in Saturn's C Ring and Cassini Division

K. Baillié

J. E. Colwell

L. W. Esposito

Mark C. Lewis
Trinity University, Mark.Lewis@trinity.edu

METER-SIZED MOONLET POPULATION IN SATURN'S C RING AND CASSINI DIVISION

KÉVIN BAILLIÉ[1,4], JOSHUA E. COLWELL[1], LARRY W. ESPOSITO[2], AND MARK C. LEWIS[3]
[1] Department of Physics, University of Central Florida, Orlando, FL 32816-2385, USA; kevin.baillie@cea.fr
[2] Laboratory for Atmospheric and Space Physics, University of Colorado at Boulder, 392 UCB, Boulder, CO 80309-0392, USA
[3] Department of Computer Science, Trinity University, One Trinity Place, San Antonio, TX 78212-7200, USA

ABSTRACT

Stellar occultations observed by the Cassini Ultraviolet Imaging Spectrograph reveal the presence of transparent holes a few meters to a few tens of meters in radial extent in otherwise optically thick regions of the C ring and the Cassini Division. We attribute the holes to gravitational disturbances generated by a population of ∼10 m boulders in the rings that is intermediate in size between the background ring particle size distribution and the previously observed ∼100 m propeller moonlets in the A ring. The size distribution of these boulders is described by a shallower power-law than the one that describes the ring particle size distribution. The number and size distribution of these boulders could be explained by limited accretion processes deep within Saturn's Roche zone.

Key words: instrumentation: photometers – methods: observational – planets and satellites: rings – space vehicles: instruments

Online-only material: machine-readable and VO tables

1. INTRODUCTION

Cassini Ultraviolet Imaging Spectrograph (UVIS) recorded more than a hundred stellar occultations since 2004 (Colwell et al. 2007, 2010; Baillié et al. 2011). Previous analyses have exploited the high spatial resolution of these occultations to study small clumps in the F ring (Esposito et al. 2008; Meinke et al. 2012) and the radial shape of ring edges (Jerousek et al. 2011). Here we report on the result of a systematic search for small gaps or openings in the rings on the scale of the resolution limit of the experiment (∼10 m). We propose that they are the azimuthally limited gaps opened up by the gravitational perturbations of an unusually large ring particle or clump of particles among the background population of particles. The holes are thus tracers of otherwise unseeable objects, and we call these gaps "ghosts." The F ring clumps (dubbed "cats" by Esposito et al. 2008) are the products of accretion in the complex F ring region near Saturn's tidal accretion limit. The holes we observe may also ultimately be the product of accretion.

While embedded objects may be found throughout the rings, because of practical limitations on the detectability of these features (discussed below) we will focus our attention here on the more opaque parts of the C ring and Cassini Division.

In Section 2 we describe the observations and our search process in detail. In Section 3 we present a moonlet perturbation model to explain the ghosts, and in Section 4 we discuss our interpretation of these data.

2. OBSERVATIONS

2.1. Cassini UVIS Data

The UVIS instrument measures a photon count rate that fluctuates depending on the amount of ring material in the line of sight between Cassini and the star using its High Speed Photometer (HSP). Scanning the ring system, we observed isolated and high photon counts throughout the ring system.

In the absence of ring material, the average photon count rate is I_0. We consider only the 66 occultations where I_0 is greater than 20 counts per integration period of 1 ms to avoid spurious detections (the complete list of occultations analyzed and of their orbit number ("rev.") is presented in Colwell et al. 2010). The spatial resolution of our data in the radial direction (corresponding to an integration period of 1 ms) is a few meters, depending on the geometry of the occultation. Though our occultations cover the entire ring system, we focused on regions where the line-of-sight optical depth is of order unity. In low optical depth regions, normal statistical fluctuations in the count rate produce ghost-like signatures. This includes the C ring and Cassini Division ringlets and plateaus (whose normal optical depth is around 0.4), and we avoid regions with local disturbances from known waves or structures in these regions described in Baillié et al. (2011). Occultations observed at low elevation angle above the ring plane also make it possible to detect ghosts in regions with smaller values of the normal optical depth due to a relatively high line-of-sight optical depth. The A ring is not included because the ubiquitous self-gravity wakes are separated by ghost-like gaps (Colwell et al. 2006, 2007; Hedman et al. 2007). We also searched the B ring. The presence of self-gravity wakes also complicates the identification of ghosts there. A prominent propeller structure in the B ring was reported by Sremcevic et al. (2011) and will be described elsewhere. As discussed above, our search focuses on the plateaus in the Cassini Division and in the C ring. We exclude regions containing the waves reported in Baillié et al. (2011), such as plateaus P5, P6, P7 and P10 (Colwell et al. 2009b).

2.2. Detection and Identification Criteria

We have developed an automated process for detecting isolated peaks in photon counts where the observed photon count rate is similar to that found in places without much ring material. In order to detect the points that present much higher photon counts than their neighboring environment, we start by smoothing the occultation signal over 10 samples and subtracting the smoothed data from the original signal (Figure 2). We arrived at a smoothing width of 10 samples

[4] Laboratoire AIM, Université Paris Diderot/CEA/CNRS, F-91191 Gif sur Yvette, France.
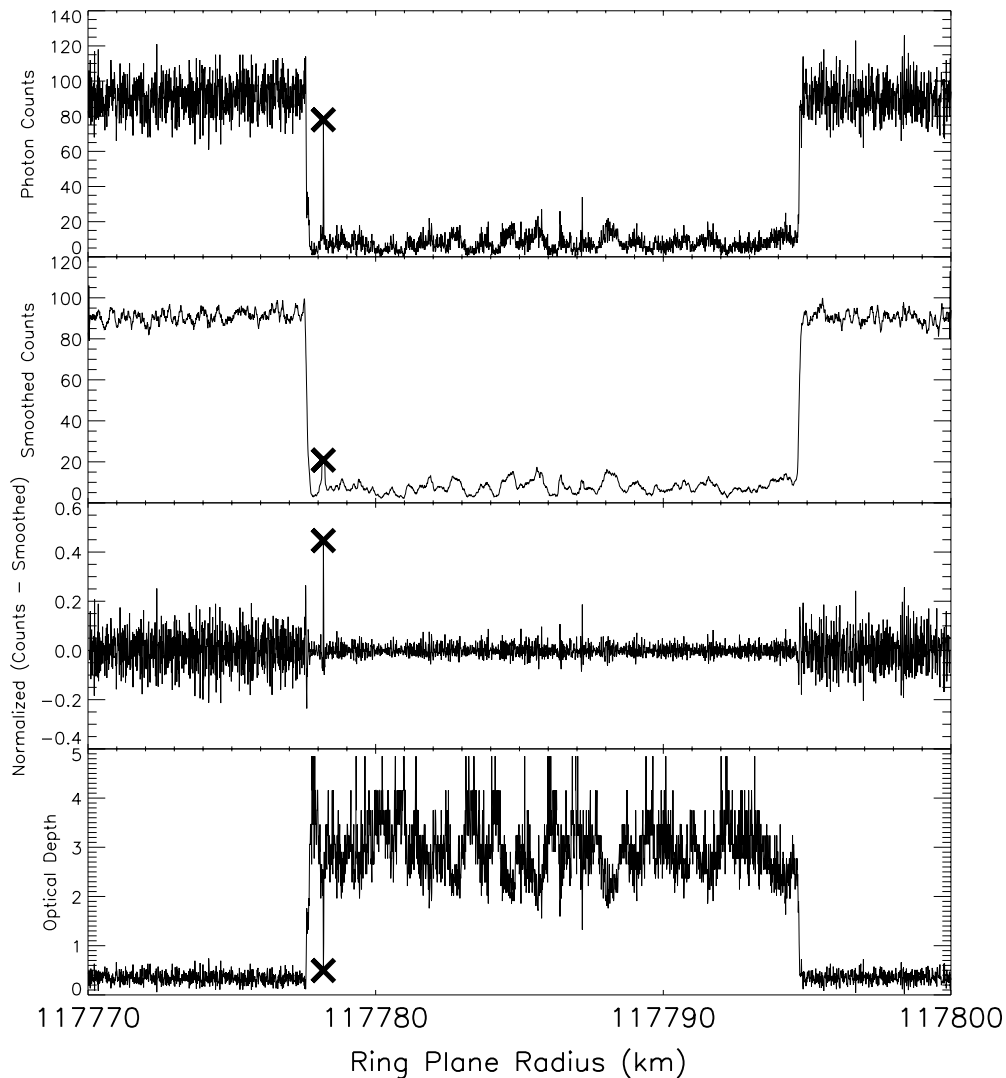
Figure 1. Analysis of a stellar occultation. Upper panels show raw photon count rates vs. ring plane radius for the occultation of the star κ Centauri. We observe the photon count rate of the star on each side of the dense Huygens ringlet. The central peak (marked by an X) matches the level of the star. The three lower panels provide details about the detection process steps: smoothing, subtracting (and normalizing by the unocculted level), and filtering on normal optical depth levels.

through trial and error analysis of the data to flag ghosts that had been previously identified by eye. Then, we flag drops in normal optical depth that are bigger than a factor of 0.9 (validated by a series of test runs on a set of visually identified ghosts). We then identify the features that present a photon count rate within 35% of the level of the star (or to the level of one of the stars, in a binary star). This whole detection process is presented in Figure 1. Binning the original signal and repeating the same process described above on the binned data set allows the identification of wider structures. We binned our data by every number of points up to 20 before removing redundant detections.

Some occulted stars, such as α Virginis and α Crucis, are actually binary stars. Depending on the projected separation of the stars in the ring plane, the step width at edges in the rings may vary according to the projection angle. For these binary stars, stellar photon count levels are additive and it can happen that one star out of the two is occulted while the other is not. The two different star levels are measured at ring edges (Figure 2). A ghost in the rings could actually present a photon count rate which matches one of the steps but not the total brightness, as shown in Figure 2.

This procedure permitted the identification of 35 ghost structures located in the C ring plateaus (all of them being five data points wide or less) and 229 in the Cassini Division that are narrower than eight data points, similarly to the identification shown in Figure 3.

We note that structures that are wider than eight points appear to be qualitatively different than narrower holes: in particular, they are not totally transparent and we can distinguish some internal structure to the almost-transparent hole (Figure 4). No completely empty gaps or ghost features are observed that are more than eight points wide. The structure widths in number of data points are reported in Table 1.

Figure 5 presents the cumulative distribution of these widths in terms of number of data points.

The 229 ghosts in the Cassini Division Ringlets and Plateaus are mainly in the Huygens Ringlet, the Triple Band and the Cassini Division ramp as shown in Figure 6.

These ghosts do not appear at the same radial locations in different occultations, showing that the holes are not axisymmetric gaps such as those opened by moons and resonances elsewhere in the rings. As shown in Figure 7, a typical feature is a few data points wide, and we characterize its width by taking the width
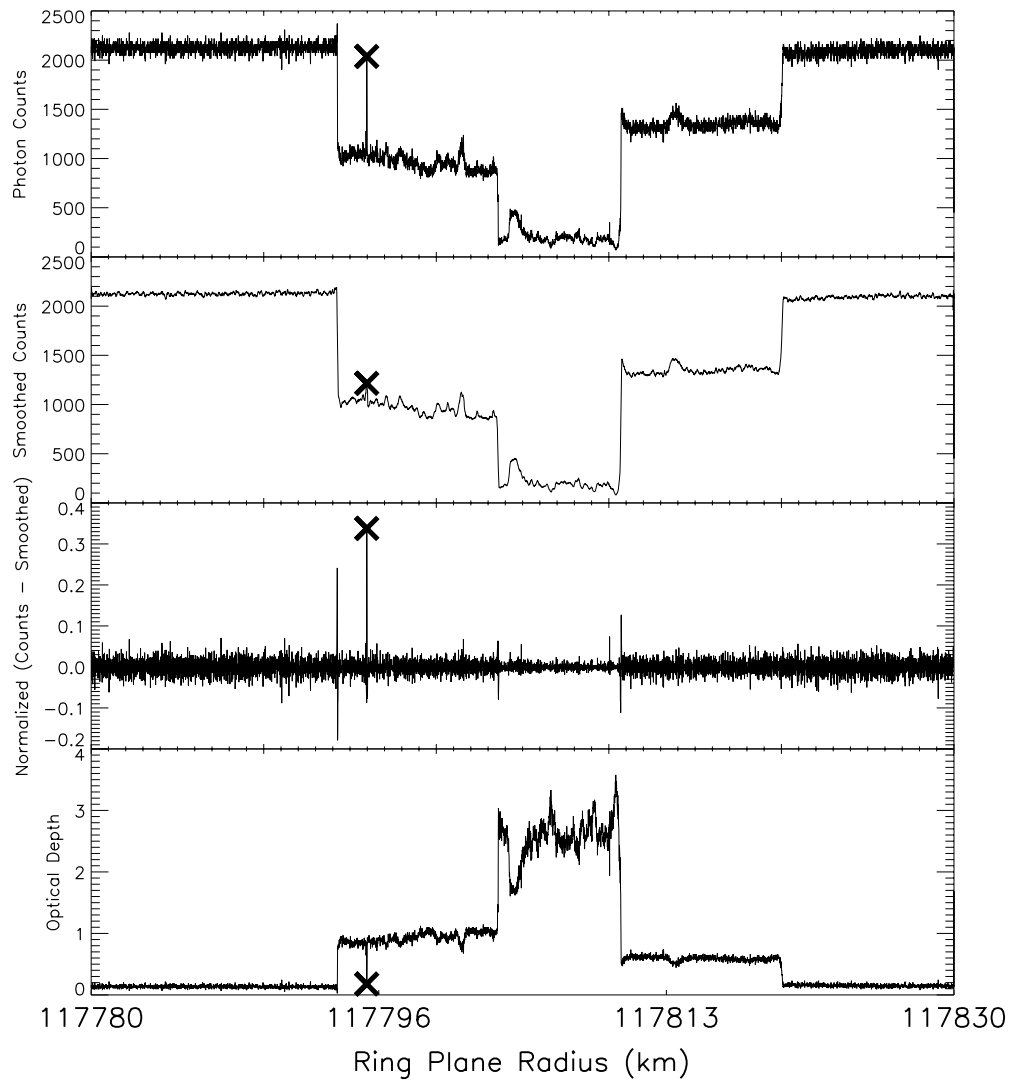
Figure 2. Binary stellar occultation. Upper panels show raw photon count rates vs. ring plane radius for the occultation of the binary star α Crucis, at the location of the dense Huygens ringlet. We observe the two rate levels for each star in the system at the edge. The central peak (marked by an X) matches the level of one of the stars. The three lower panels provide details about the detection process steps: smoothing, subtracting (and normalizing by the unocculted level), and filtering on normal optical depth levels.
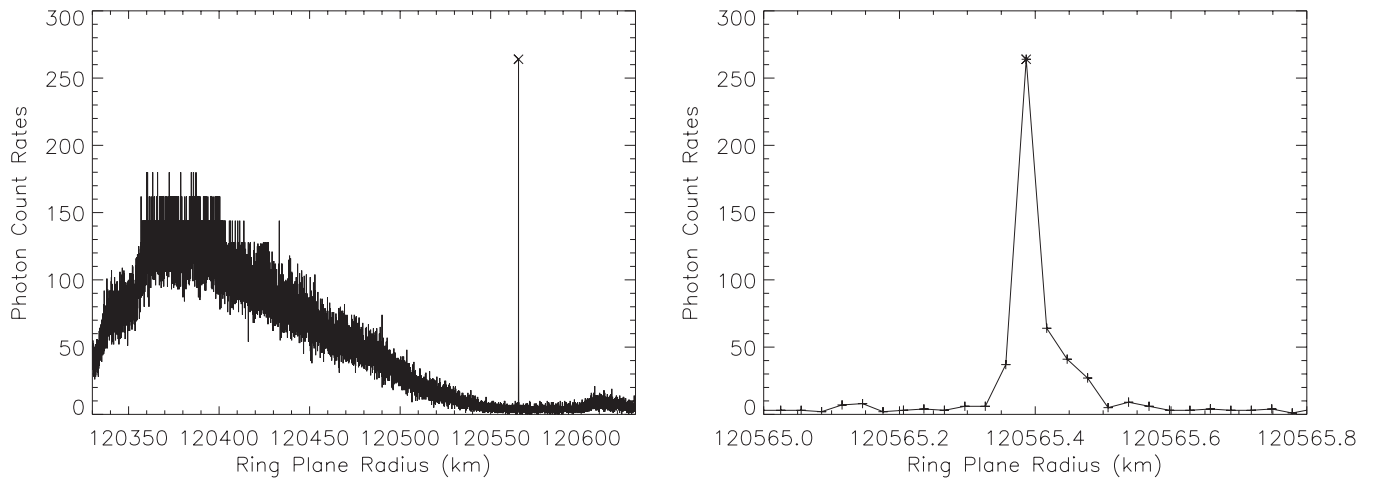

Figure 3. The Cassini Division Triple Band. Photon count rates from the occultation of ζ Orionis, rev. 47, across the "Triple Band" (Colwell et al. 2009b) of the Cassini Division (120,550 km to 120,800 km).

Table 1
Detected Ghost Rates and Widths

Width N	C Ring		Cassini Division	
(in Data Points)	Number of Ghosts	Width W (m)	Number of Ghosts	Width W (m)
1	17	5.4–46.7	105	1.7–82.6
2	11	6.7–41.8	61	2.4–94.3
3	5	10.4–15.6	32	3.8–193
4	0	⋯	11	5.2–184
5	2	18.8–26.5	8	5.0–277
6	0	⋯	7	27.9–149
7	0	⋯	5	37.4–85.8
⩾8	0	⋯	36	53.5–375

Notes. Widths are provided in data points N (number of data points with higher photon counts than the width at half height of the hole) and converted to meters (W), using the occultation resolution. Considering a width-uncertainty of one data point on our measure of the ghost's width, this corresponds to an uncertainty of W/N meters or a relative uncertainty of $1/N$. A complete table of the observed features and their locations is provided in the Appendix.
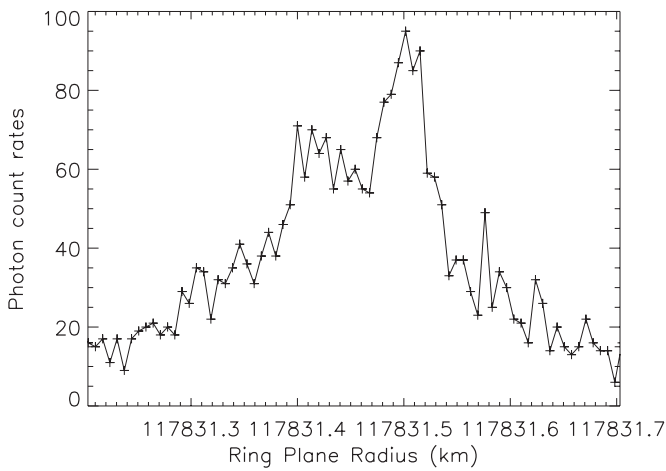

Figure 4. Substructures in a ghost wider than eight points can be identified in the photon count rates from the β Centauri occultation (rev. 96). The background level of the star is normalized at 100. These wider structures are not completely transparent and are not included in this analysis.

at half-height of a linear interpolation of the occultation scan (Table 1 and Figure 5 show the width distribution in terms of number of data points). The widths of these gaps are 5.4–47 m in the C ring and 1.7–280 m in the Cassini Division.

2.3. False Detections

Cosmic rays or electronic transients can produce a single measurement with a high photon count rate. We verify that our ghosts are not due to cosmic rays or other artifacts using the following statistical analysis. In regions of zero optical depth, we expect the photon count rate to be close to the level of the unocculted star: we can model our data as a Poisson distribution with a mean equal to the signal mean. Therefore, we can estimate the probability that significantly higher counts than a particular measured value belong to this distribution. If they appear unlikely to belong to this distribution, we count them as artifacts (i.e., cosmic ray hits). We use the Huygens and Encke gaps, and the Roche division to determine the frequency of cosmic ray or other anomalous high signals in HSP data. For each occultation, and for each of these gaps, we measure the mean photon count rate. We verified that our signal in this region can be considered as a Poisson distribution by comparing the mean of the signal with the variance of the signal. We find that
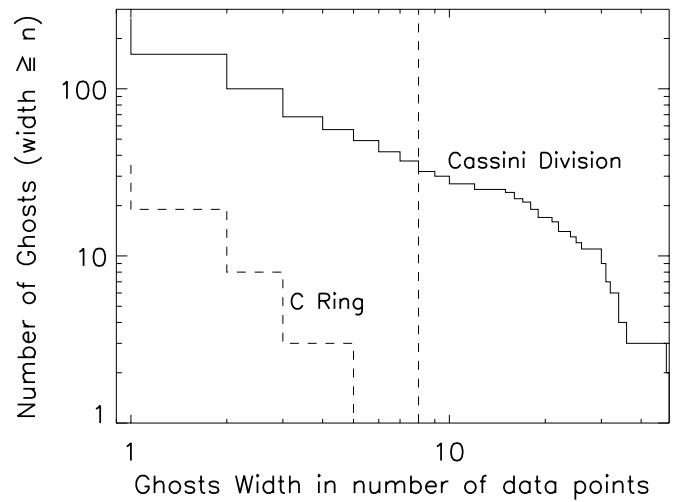

Figure 5. Cumulative width distribution of the detected ghosts in number of data points in the C ring (dashed curve) and in the Cassini Division (solid curve). The zone at the left of the vertical dashed line delimits the structures that we consider as ghosts with a high confidence. Larger structures (wider than eight data points) that can correspond to other phenomena are excluded from the following study. Nevertheless, there is no strong inflection in the shape of the distribution at our selected cutoff of eight points showing that our conclusions are not influenced by the precise value of this cutoff.

the data in the ring gaps identified above are indeed consistent with Poisson statistics.

Then, considering a Poisson distribution, we estimate $p(k, \mu)$, the probability of obtaining a detection rate k:

$$p(k, \mu) = \frac{e^{-\mu} \mu^k}{k!}. \tag{1}$$

Thus, the probability of measuring a photon count rate $\geqslant k$ is:

$$P(k, \mu) = 1 - \sum_{x=0}^{k-1} (p(x, \mu)) \tag{2}$$

and the number m of points at this level that can be expected in a Poisson distribution of N points, is given by Colwell (1989):

$$m(k, \mu) = N P(k, \mu) = N \left(1 - \sum_{x=0}^{k-1} (p(x, \mu)) \right). \tag{3}$$
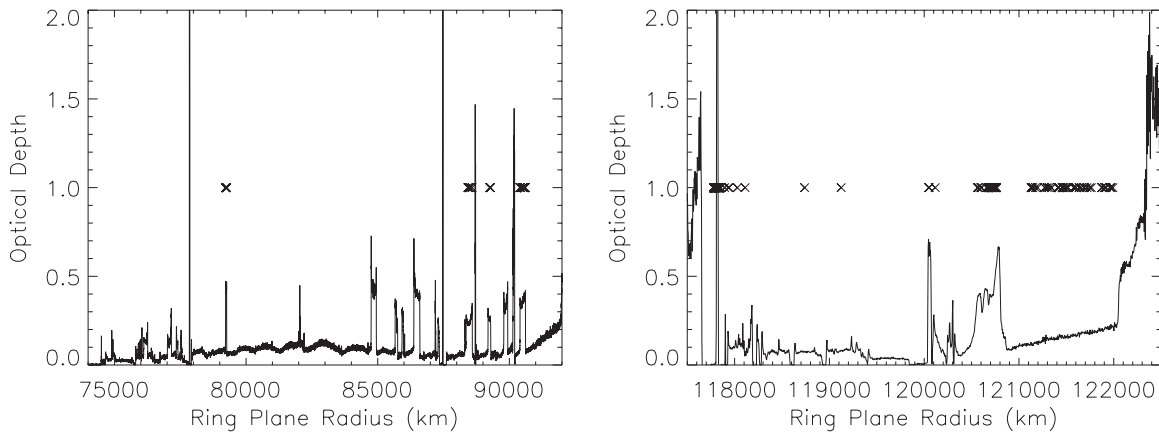
Figure 6. Radial distribution of the ghost observations (x symbols) in the C ring (left) and the Cassini Division (right). Reported ghost observations are plotted over normal optical depth profiles of the two regions. Ghosts are detected in regions of intermediate line-of-sight optical depth (see Section 2), so some ghosts are detected in regions of low normal optical depth in occultations with a small elevation angle above the ring plane.
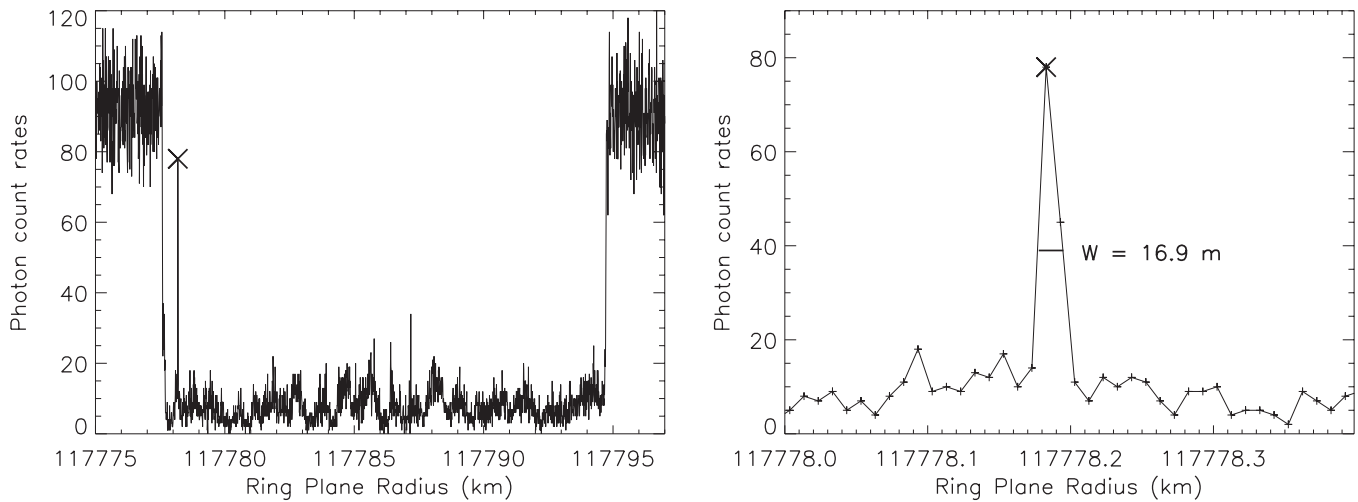

Figure 7. A ghost in the Huygens Ringlet. Photon count rates from the occultation of κ Centauri, rev. 35 across the Huygens Ringlet (left). We measure the width of the isolated peak (here defined by two data points) by estimating the width at half-height of the interpolation of the data (16.9 m with an 8 m uncertainty) (right).

We considered a measured value to be an artifact if $m < 0.01$. Applying this process to all our identified potential artifacts allowed us to clearly identify 17 artifacts out of 8.43×10^7 measurements. Therefore we derived a density of anomalous measurements of 1 artifact per 4.96×10^6 points. We compare this density with the number of identified ghosts that are one data point wide: 122 one data point wide ghosts were found out of 70 million scanned points. According to our artifact frequency, we should expect to find 14 artifacts in our data set if we had not already been filtering our ghost detection by matching the background level of the star (and therefore excluding all potential artifacts for which counts would be significantly higher than the background level of the star). This number therefore overestimates the number of our ghosts that could be artifacts. An analysis of other UVIS data described in Chambers et al. (2008) found only 1 artifact in 1.3×10^8 measurements. (That analysis studied data with much lower mean signal levels than the star signals in the gaps analyzed here. The higher artifact detection rate we find here is likely due to this difference in overall signal level, but we do not have a model for what produces these artifacts because cosmic ray rates should be the same between the two analyses.) According to that estimation, the actual number of our ghosts being artifacts should be negligible and we can state with a good confidence that our observed ghosts that are one data point wide

are actual structures in the rings and not due to cosmic rays or other electronic transients. In addition, wider holes cannot statistically be explained by the coincidence of two or more consecutive artifacts in the data set.

3. SINGLE PERTURBER MODEL

The observed features described above appear to represent nearly empty gaps in the rings. Since they are not always found at the same locations, and we have deliberately avoided regions disturbed by waves or self-gravity wakes, we conclude that these gaps are most likely due to gravitational perturbations in the ring material caused by isolated massive perturbers. Models show that depletion zones are formed on the outer trailing and inner leading sides of an embedded massive object inside the rings (Petit & Henon 1988; Spahn & Wiebicke 1989; Spahn et al. 1992; Spahn & Sremčević 2000; Sremčević et al. 2002; Seiß et al. 2005). In the A ring, where similar depletion zones have been observed, the two-lobed signature produced by a moonlet resembles a two-bladed propeller, so the disturbing mass is called a propeller moonlet by Spahn & Sremčević (2000).

The Hill sphere of a boulder (larger-than-average ring particle) of mass $M_{boulder}$ and of semi-major axis $a_{boulder}$ is given by $r_H = a_{boulder}(M_{boulder}/3M_{Saturn})^{1/3}$, where M_{Saturn} is Saturn's
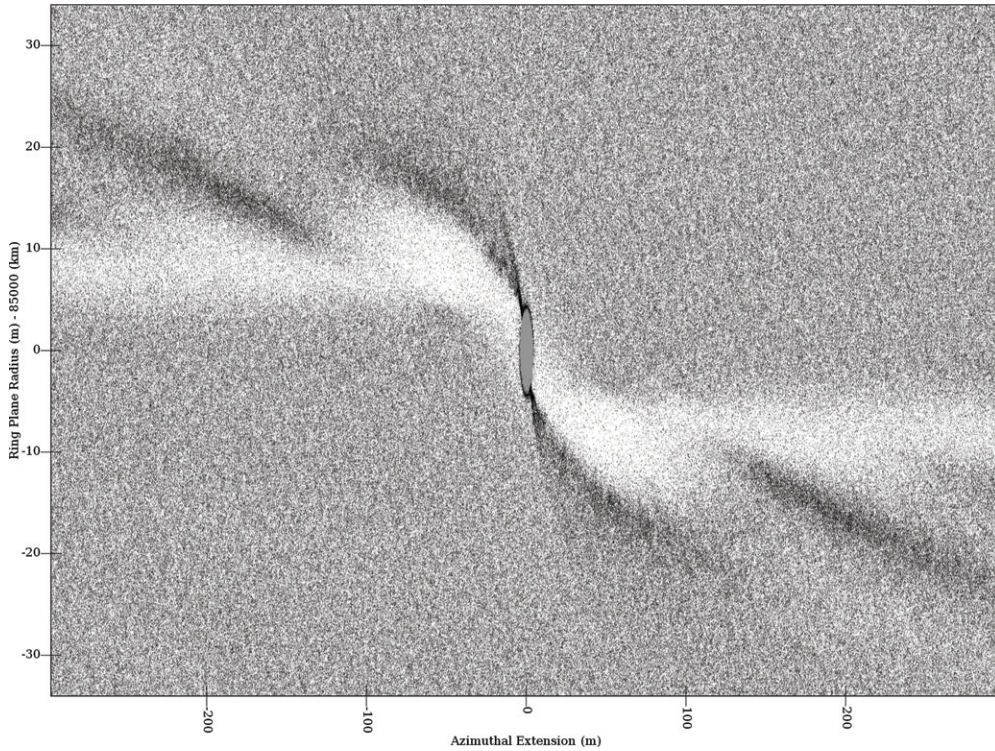
Figure 8. Propeller signature for a 5 m radius boulder. The boulder is located at (0, 0) and the orbital direction is from left to right. Particle radius ranges from 5.1 cm to 10.2 cm following a power law distribution with cumulative index $Q = 2$. The optical depth is set to 0.4 and the surface mass density to 2.0 g cm^{-2}.

mass. The most recent numerical simulations from Tiscareno et al. (2008), Lewis & Stewart (2009) and Tiscareno et al. (2010) use numerical integration of the classical Hill problem (massless test particles orbiting a large central body and deflected in the vicinity of a perturbing mass) in order to model propeller signatures. Particles with a semi-major axis difference Δa with the boulder less than $2r_H$ are showed to follow horseshoe orbits. Particles with larger values of Δa are still perturbed and receive a kick in eccentricity proportional to $1/(\Delta a)^2$. In addition, Showalter & Burns (1982) showed that the phases of these particles' orbits are roughly aligned. These now-eccentric particles will leave open spaces downstream on the outer trailing side and inner leading side of the boulder. Figure 8 shows a simulation using the model of Lewis & Stewart (2009) with parameters chosen to represent a C ring plateau. We propose that ghosts may be detections of the nearly empty spaces immediately upstream and downstream of an unseen boulder. The numerical simulations show the same radial extent of these primary depletion zones ($\approx 3r_H$) found by Sremčević et al. (2002) and Tiscareno et al. (2008).

The azimuthal extent can be much larger. The depleted regions gradually fill in as the material drifts away from the moon due to the combined effects of collisions and interparticle gravitational forces provoking either a damping of the eccentricity, a randomizing of the phases or a scattering of the eccentric particles in the depletion zones. Both collisions and self-gravity decrease the eccentricity of the wake particles so the structures will vanish at some azimuthal distance from the boulder, although some persist for multiple synodic periods. The recent detection of propellers in the A ring raised the question of whether the bright S-shape of the propeller signature was due to the outer edge of the depletion zones or rather to the boulder wakes (Sremčević et al. 2007; Tiscareno et al. 2008). We can ignore this debate as we directly observe the gaps.

From Lewis & Stewart's (2009) numerical tests on various boulder and particle sizes, it appears that the size of the primary depletion zone (both radially and azimuthally) is not sensitive to particle size variations as long as the ring particles are at least three times smaller (assuming the same density for the particles and the boulder) than the boulder.

Previous estimates by Sremčević et al. (2002) and Tiscareno et al. (2008) stated that the radial extent of the primary lobe grows linearly with the boulder radius:

$$\Delta r \approx 3r_H. \qquad (4)$$

In addition, previous work from Spahn & Sremčević (2000) and Sremčević et al. (2002) calculated that the azimuthal extent grows as the cube of the Hill radius of the boulder and depends on the local ring viscosity $\nu_0 = 10$ cm^2 g^{-1}. Though Tiscareno et al. (2008) were unable to confirm the trends predicted by the earlier references, we will define the azimuthal extent of the primary depletion zone following Sremčević et al.'s (2002) equation with Ω_0 the boulder Keplerian angular velocity and $\beta \approx 1$:

$$\Delta \Phi \approx 50 \frac{\Omega_0 r_H^3}{(1 + \beta)\nu_0}. \qquad (5)$$

From a consideration of ring viscosity, in order for a boulder to create an opening in the ring, the boulder must provide accelerations to the background ring particles that are larger than those due to external or other internal forces. We can estimate the size of an individual boulder necessary to provide such an acceleration by considering the sizes of the particles and clumps in the background population. Unlike the A ring and B ring, where large clumps of particles are present in the form of self-gravity wakes, the C ring and Cassini Division do not show evidence of self-gravity wakes. This is not surprising given the low surface mass densities in both regions ($\sim$1–5 g cm^{-2}; Baillié
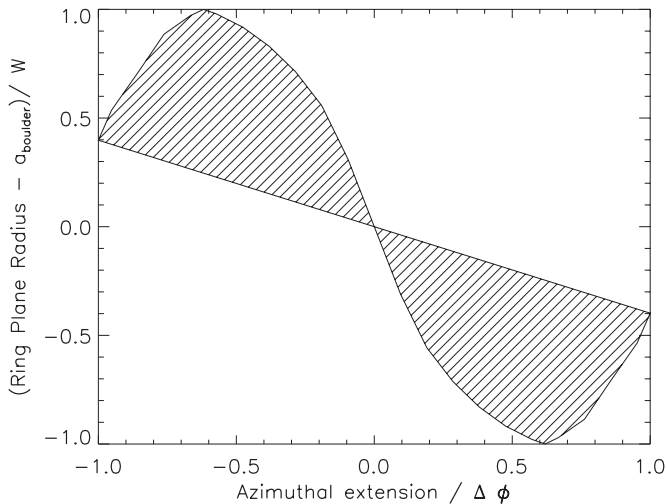
Figure 9. Modeled primary depletion zones. Distances are in units of the upper radial and azimuthal extents.

Table 2
Derived Boulder Radii

	C Ring	Cassini Division
Ghost widths—W	5.4–47 m	1.7–280 m
Boulder radii—r	1.3–12 m	0.31–49 m
Azimuthal extents Δ_Φ	64 m–49 km	1.4 m–5600 km

Notes. Derived boulder radii from the application of the propeller model to the width distribution of observed ghosts in the C ring and the Cassini Division. Inferred azimuthal extents of the propellers (estimated with a viscosity $\nu_0 = 10$ cm^2 g^{-1}) are also presented. Boulder radii are model-dependent (see below).

et al. 2011; Colwell et al. 2009a) which give a self-gravity length scale (Toomre 1964) of $\lambda_{crit} = 4\pi^2 G(\sigma/\kappa^2) \sim 1$ m, where σ is the surface-mass density and κ the epicyclic frequency. Thus, purely gravitational clumps in these regions should be no larger than ~1 m, or roughly the same scale as the largest individual particles (Zebker et al. 1985). Another estimate of the sizes of boulders necessary to open gaps comes from an estimate of the total rms velocity dispersion from the thickness of the ring. These values are ~2–4 m in the C ring plateaus (Baillié et al. 2011) and ~3–20 m in the Cassini Division plateaus (Colwell et al. 2009a). These considerations give the consistent result that boulders larger than several meters in radius will provide accelerations large enough to create depletion zones in the C ring and Cassini Division.

3.1. Boulder Size Distribution

Assuming that the ghosts observed by UVIS are part of the depletion zones created by boulders within the rings, we can estimate the Hill radii for these boulders and therefore their actual radii as reported in Table 2. The complete list of these radii for all ghosts is provided in the online journal (see Table 3). From Lewis & Stewart (2009), we can estimate the upper limits on the background particle sizes around 4 m in the C ring and up to 16 m in the Cassini Division.

In principle, we could derive estimates of the particle size distributions from these observations, but to do so we must take into account the variable spatial resolution of the occultations: even though the UVIS instrument has a constant integration time, each occultation has a different spatial resolution in the ring plane. This complicates the interpretation of our width
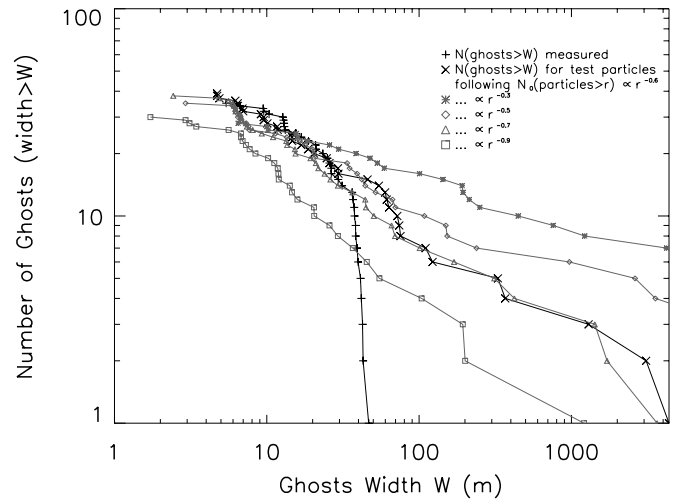

Figure 10. Cumulative size distributions of the ghosts. Observed (+ symbols) and best-modeled (× symbols) holes are displayed for the C ring. The initial boulder size distributions at the origins of the modeled ghost populations follow power-law distributions with cumulative power-law indices of 0.6. Fits to the data with different power-law indices are also shown to illustrate the sensitivity of the model to the particular power-law index chosen.

measurements. In order to estimate the impact of this variability and in order to model the difference between the observable widths and the observed widths, we use a Monte Carlo algorithm designed to model the statistical impact of our occultation resolution variations. This algorithm evaluates the modeled observed ghost widths from a known particle size distribution. From an arbitrary proportion of the total number of particles, we estimate the corresponding particle radius and model the Hill radius of the boulder and the maximal width of the ghost that would be created (see Equation (4) above; also Spahn & Sremčević (2000), Sremčević et al. (2002), and Tiscareno et al.'s (2008) numerical simulations results). We assume each boulder produces a pair of gaps with a maximal radial width Δr given by Equation (4), an azimuthal extent $\Delta\Phi$ given by Equation (5) and a shape modeled in Figure 9.

We assume that this hole is on a random occultation track, at a random azimuthal distance from the boulder (within the range of the primary open gap), and we estimate what would be measured for its width given the occultation resolution and based on our 13 point interpolation model of the primary depletion zone width as a function of radial distance from the boulder. However, a precise study of the density of such particles would require a much more complete model of the primary, secondary and subsequent depletion zones (by order of distance from the boulder), with estimated probabilities of encounters with random background particles. Such a model would require ray tracing simulations which are left for a future study. The statistical repetition of this process allows us to determine a cumulative size distribution of the theoretically observed ghost widths. We assume that the boulder size distribution in the C ring and the Cassini Division can be modeled as a power-law. By comparing this distribution with the measured ones, we adjust the initial particle size distribution index in order to match the observed one. The cumulative boulder size distributions that best reproduce (χ^2 minimization) the observed ghost width distributions are $N(\geqslant r) \propto r^{-Q}$, with $Q_{C\,ring} = 0.6$ in the C ring and $Q_{CD} = 0.8$ in the Cassini Division (Figures 10 and 11), where $N(\geqslant r)$ is the number of particles with a radius larger than r. The difference between these indices is of the same order of magnitude as the

Table 3
Detected Ghosts

Stellar Occultation	Ring Plane Radius	Width		Moonlet Radius	Azimuthal Extension
	(km)	(Data Points)	(m)	(m)	(m)
α Vir (34)	79230.1	2	41.2	10.9	33526.9
α Vir (34)	79232.7	2	38.3	10.1	26963.1
126 Tau (8)	79233.1	2	6.7	1.8	142.6
α Vir (34)	79235.3	1	29.4	7.7	12199.9
126 Tau (8)	79240.1	3	10.3	2.7	530.9
α Vir (34)	79241.7	1	31.2	8.2	14575.6
α Vir (34)	79245.7	1	25.0	6.6	7473.3
α Vir (30)	79246.2	1	36.8	9.7	23899.9
α Vir (30)	79252.3	1	46.7	12.3	48647.3
α Vir (34)	79255.0	2	41.8	11.0	34860.6

Notes. Widths are provided in data points N (number of data points with higher photon counts than the width at half height of the hole) and converted in meters, using the occultation resolution. Considering a width uncertainty of one data point on our measure of the ghost's width, this corresponds to an uncertainty of W/N meters or a relative uncertainty of $1/N$. Their locations are presented with the moonlet radius that could be at the origin of these features and the modeled azimuthal extensions of the features.

(This table is available in its entirety in machine-readable and Virtual Observatory (VO) forms in the online journal. A portion is shown here for guidance regarding its form and content.)
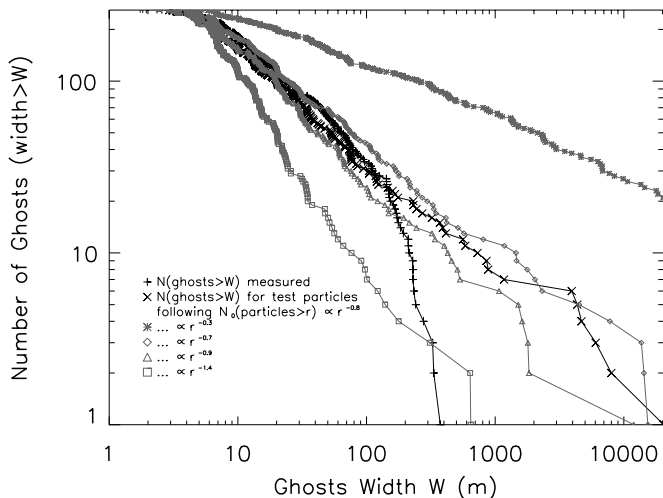

Figure 11. Cumulative size distributions of the ghosts. Observed (+ symbols) and best-modeled (× symbols) holes are displayed for the Cassini Division. The initial boulder size distributions at the origins of the modeled ghost populations follow power-law distributions with cumulative power-law indices of 0.8. Fits to the data with different power-law indices are also shown to illustrate the sensitivity of the model to the particular power-law index chosen.

difference between the distributions of smaller particles given in Zebker et al. (1985): $Q_{C\,ring} = 2.1$ and $Q_{CD} = 1.75$. These derived indices suggest that the boulder population follows a different size distribution from the rest of the ring particles. We should however note that the precision on the estimation of the C ring power-law index is lower than the Cassini Division one due to the smaller number of ghosts in the C ring. The optimal power-law models for the boulder size distribution shown in Figures 10 and 11 predict an excess of gaps larger than 200 m in the Cassini Division and larger than 40 m in the C ring. However, this prediction is based on the assumption that the boulder size distribution has no upper limit. The observed rapid fall-off in the number of putative boulders larger than a few tens of meters may therefore be indicative of the upper limit of the boulder population size distribution. That is, the data suggest that the size distribution of boulders argued for here does not extend up to the size of the propeller objects observed in the A ring and is

instead truncated at 35 m in the Cassini Division and 10 m in the C ring.

4. DISCUSSION

The size distribution of the observed boulders is described by a shallower power-law than the one that describes the ring particle size distribution. Since the boulders are observed in widely separated regions within the C ring and Cassini Division, we do not propose that each population is derived from fragmentation of a single parent object. In addition, we would expect the resulting particle size distribution from a fragmentation process to be steeper than our derived boulder size distributions. The size distributions produced by fragmentation of asteroids, glacial boulders, and indeed the main rings of Saturn have $Q = 1.5$–2.5 (Hartmann 1969; Dohnanyi 1969, 1972; Gladman et al. 2009; Zebker et al. 1985). The Cassini RSS data also show that the size distribution has a sharp cut-off at a few meters (Marouf et al. 2012), where the particle size distribution becomes even steeper and less consistent with our distribution.

Since Cassini's arrival in Saturn's orbit, the particle size distribution had to be extended to larger sizes: recent observations of the A ring propellers (Tiscareno et al. 2006, 2008, 2010; Sremčević et al. 2007; Lewis & Stewart 2009) lead to a steeper distribution of the largest particles, modeled as a power-law distribution with a cumulative index $Q \sim 5$ (Tiscareno et al. 2010). This distribution is also steeper than our C ring and Cassini Division results. Lewis & Stewart (2009) introduced the idea of a break in the power-law distribution and suggested that the A ring propeller population could be a bump in the particle size distribution formed by accretion inside the planet Roche radius as detailed in Figure 3 from Canup & Esposito (1996): accretion can produce a shallower size distribution as small particles are removed from the distribution and incorporated into larger particles (see also Bodrova et al. 2012). We may be seeing evidence of such a phenomenon in the ghosts reported here.

Our results may also be compared to the F ring clumps and moonlets observations from Esposito et al. (2008) and Meinke et al. (2012): UVIS occultations showed a flatter particle-size-distribution extension to larger sizes than estimated from radio-occultations. However, though the presence of the F ring

moonlets could be interpreted as evidence for the evolutionary models involving accretion and disruption mechanisms described in Barbara & Esposito (2002), neither the F ring clumps distribution nor our C ring and Cassini Division results look similar to the bimodal distribution in the Barbara & Esposito (2002) model. The F ring clumps are mostly elongated temporary aggregates that may be more abundant and hide the solid bodies predicted by this model.

It is worth noting that the objects inferred in the C ring are smaller than the ones in the Cassini Division, which is consistent with stronger tidal forces closer to Saturn, therefore making accretion more difficult closer to the planet. Our spatial resolution is generally better in the Cassini Division than in the C ring which makes detection of smaller holes in the Cassini Division easier. The smaller hole sizes in the C ring are therefore real and not due to observational bias. Analysis of density waves by Baillié et al. (2011) indicates that the largest particles in the C ring are smaller than those in the Cassini Division as well.

Our boulders constitute evidence of a distinct population of bigger particles (reaching a few m in the C ring and up to a few tens of meters in the Cassini Division) that do not appear to be obtained by extrapolation of the previous particle size distribution models. However, our model considers the ghost as the optimal signature of a primary depletion zone taken at the longitude where it is largest. Therefore, the derived particle radius should better be considered as a lower value for a particle able to create such a hole. Furthermore, our derived boulder sizes are based on numerical simulations with a number of simplifications and assumptions about the background population. In the lower part of the boulder size distribution (less than a few times the size of the background ring particles), it is reasonable to think that only partial or less defined gaps might be opened, leading to a shallower gap width distribution than for bigger boulders. Therefore, the original smaller boulder size distribution could be steeper than the derived best model from Figures 10 and 11. The distribution of boulder sizes is distinct from the background population, but due to limitations of our data and the model, we cannot make more precise conclusions about the absolute number and sizes of the boulders.

This raises the question of a possible different origin between the background ring particles and the boulders. We previously ruled out a fragmentation scenario that would generate a much steeper distribution of the boulders and that would not produce a population of larger objects with a break in size to the next largest objects. Karjalainen & Salo (2004) and Meinke et al. (2012) showed that an accretion scenario, on the other hand, could form transient aggregates inside the Roche limit, which would disturb the encountering particles and clear depletion zones: accretion could lead to significantly larger boulders than the next largest objects in the population that feeds accretion. In addition, the small size of the boulders is consistent with frustrated accretion in the Roche zone, and the smaller size of the boulders in the C ring than the Cassini Division is consistent with tidally frustrated accretion.
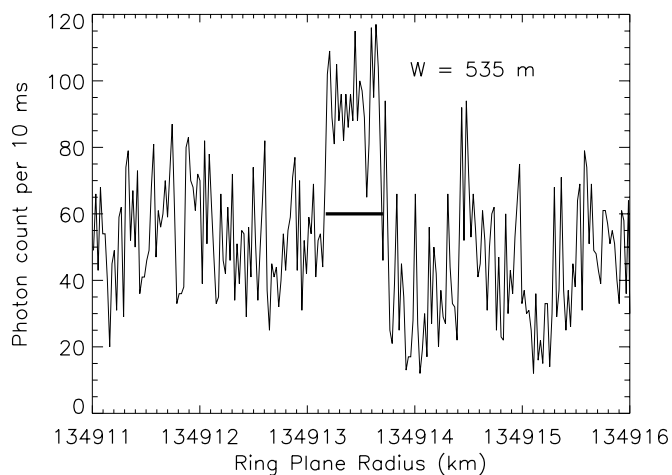
Figure 12. The Blériot propeller object. Photon count rates from the ζ Persei occultation (rev. 42) showing the Blériot Propeller Object. We measure a width of 535 m.

APPENDIX

A.1. Detected Ghosts

A.2. UVIS Observation of the Blériot Propeller Object

Recent observations by Tiscareno et al. (2006, 2008, 2010), Sremčević et al. (2007), and Lewis & Stewart (2009) described propellers in the A ring, such as the Blériot Propeller Object for example. As the occultation of ζ Orionis crossed its location, we were able to observe this object in UVIS data (Figure 12). We could estimate the radius of the Blériot Propeller Object to be ∼83 m, which corresponds to a lower estimate from imaging measures by Tiscareno et al. (2010). We can explain the variations with their other measures by the fact that it is highly improbable that we scanned the propeller at the azimuth where it was the largest.

REFERENCES

Baillié, K., Colwell, J. E., Lissauer, J. J., Esposito, L. W., & Sremčević, M. 2011, Icar, 216, 292
Barbara, J. M., & Esposito, L. W. 2002, Icar, 160, 161
Bodrova, A., Schmidt, J., Spahn, F., & Brilliantov, N. 2012, Icar, 218, 60
Canup, R. M., & Esposito, L. W. 1996, Icar, 119, 427
Chambers, L. S., Cuzzi, J. N., Asphaug, E., Colwell, J., & Sugita, S. 2008, Icar, 194, 623
Colwell, J. E. 1989, PhD thesis, Colorado Univ., Boulder
Colwell, J. E., Cooney, J. H., Esposito, L. W., & Sremčević, M. 2009a, Icar, 200, 574
Colwell, J. E., Esposito, L. W., Jerousek, R. G., et al. 2010, AJ, 140, 1569
Colwell, J. E., Esposito, L. W., & Sremčević, M. 2006, GeoRL, 33, L07201
Colwell, J. E., Esposito, L. W., Sremčević, M., Stewart, G. R., & McClintock, W. E. 2007, Icar, 190, 127
Colwell, J. E., Nicholson, P. D., Tiscareno, M. S., et al. 2009b, in Saturn from Cassini-Huygens, ed. M. K. Dougherty, L. W. Esposito, & S. M. Krimigis (Dordrecht: Springer), 375
Dohnanyi, J. S. 1969, JGR, 74, 2531
Dohnanyi, J. S. 1972, Icar, 17, 1
Esposito, L. W., Meinke, B. K., Colwell, J. E., Nicholson, P. D., & Hedman, M. M. 2008, Icar, 194, 278
Gladman, B. J., Davis, D. R., Neese, C., et al. 2009, Icar, 202, 104
Hartmann, W. K. 1969, Icar, 10, 201
Hedman, M. M., Burns, J. A., Showalter, M. R., et al. 2007, Icar, 188, 89
Jerousek, R. G., Colwell, J. E., & Esposito, L. W. 2011, Icar, 216, 280
Karjalainen, R., & Salo, H. 2004, Icar, 172, 328
Lewis, M. C., & Stewart, G. R. 2009, Icar, 199, 387

Marouf, E. A., Wong, K., French, R., & Rappaport, N. 2012, in AAS/Division for Planetary Sciences Meeting Abstracts, Vol. 44, 501.03

Meinke, B. K., Esposito, L. W., Albers, N., & Sremčević, M. 2012, Icar, 218, 545

Petit, J., & Henon, M. 1988, A&A, 199, 343

Seiß, M., Spahn, F., Sremčević, M., & Salo, H. 2005, GeoRL, 32, 11205

Showalter, M. R., & Burns, J. A. 1982, Icar, 52, 526

Spahn, F., Saar, A., Schmidt, S., & Schwarz, U. 1992, Icar, 100, 143

Spahn, F., & Sremčević, M. 2000, A&A, 358, 368

Spahn, F., & Wiebicke, H. 1989, Icar, 77, 124

Sremcevic, M., Esposito, L. W., Colwell, J. E., & Albers, N. 2011, in EPSC-DPS Joint Meeting 2011, 1616

Sremčević, M., Schmidt, J., Salo, H., et al. 2007, Natur, 449, 1019

Sremčević, M., Spahn, F., & Duschl, W. J. 2002, MNRAS, 337, 1139

Tiscareno, M. S., Burns, J. A., Hedman, M. M., & Porco, C. C. 2008, AJ, 135, 1083

Tiscareno, M. S., Burns, J. A., Hedman, M. M., et al. 2006, Natur, 440, 648

Tiscareno, M. S., Burns, J. A., Sremčević, M., et al. 2010, ApJL, 718, L92

Toomre, A. 1964, ApJ, 139, 1217

Zebker, H. A., Marouf, E. A., & Tyler, G. L. 1985, Icar, 64, 531